

# Stress-Strain Behavior of Sands Cemented by Microbially Induced Calcite Precipitation

B. M. Montoya, M.ASCE<sup>1</sup>; and J. T. DeJong, M.ASCE<sup>2</sup>

**Abstract:** Microbial induced calcite precipitation (MICP) is a novel biomediated ground improvement method that can be used to increase the shear strength and stiffness of soil. The evolution of the shear strength and stiffness of sand subjected to undrained and drained shearing is evaluated using triaxial tests. MICP treated sands with cementation levels ranging from young, uncemented sand to a highly cemented sandstonelike condition are subjected to undrained shear. A transition from strain hardening to strain softening behavior and a corresponding transition of global to localized failure as cementation is increased is observed. Moderately cemented specimens are subjected to various stress paths, which result in a change to the shear strength and volumetric behavior. Shear wave velocity is used to nondestructively monitor the change in small-strain stiffness during shearing, which provides an indication of cementation degradation as a function of strain level. Because shear wave velocity is influenced by both the level of cementation and the change in effective mean stress during shearing, the normalized shear modulus is used to evaluate the degradation of cementation during shearing. DOI: 10.1061/(ASCE)GT.1943-5606.0001302. © 2015 American Society of Civil Engineers.

**Author keywords:** Cemented sand; Shear strength; Shear wave velocity; Microbial induced calcite precipitation; *Sporosarcina pasteurii*; Urea hydrolysis.

## Introduction

Continued rehabilitation and expansion of civil infrastructure are required to meet growing societal needs; however, infrastructure development is often limited by incompetent soil conditions upon which to found structures. Ground improvement can improve soils to support new or rehabilitated infrastructure, with conventional methods including densification of soil with mechanical energy or injecting a binding agent such as cement, epoxy, or silicates (Karol 2003). However, biologically based alternative techniques have emerged that may provide a more natural and sustainable solution (Mitchell and Santamarina 2005; Ivanov and Chu 2008; DeJong et al. 2013). These techniques utilize biological metabolic processes to mediate improvement of soil properties (e.g., strength and stiffness) (DeJong et al. 2010, 2011). Microbial induced calcium carbonate precipitation (MICP) (referred to herein as calcite precipitation to be consistent with the MICP terminology and previous literature) is a natural biologically mediated method to create cementation in situ and improve mechanical soil properties (Chou et al. 2011; van Paassen et al. 2010; Whiffin et al. 2007; DeJong et al. 2006). The MICP process presented herein utilizes urea hydrolysis as the biochemical reaction to increase the alkalinity of the pore fluid and induce calcite precipitation (Fujita et al. 2008; Stocks-Fischer et al. 1999). *Sporosarcina pasteurii*, a common alkaliphilic soil bacterium with a high urease activity, was used to facilitate the biochemical reaction that induced cementation (Mortensen et al. 2011).

The improvement of strength and stiffness of the MICP treated soil is influenced by both the densification and bonding effects of the mineral precipitation (DeJong et al. 2010). The induced calcite precipitation occupies void space within the soil matrix, effectively reducing the void ratio and densifying the soil. If the precipitated calcite was debonded from the sand grains and yet remained in the pore space as calcite fines, the resulting soil would be expected to exhibit a higher undrained shear strength than that of an untreated sand. If the bonding effect from the precipitation is considered in addition to the densification effect, an even larger undrained shear strength and higher stiffness is achieved. The improvement of the strength and stiffness of MICP treated soil also depends on the precipitation level; additional precipitated calcite results in a further densification and cementation at particle-particle contacts.

In the study presented herein the evolution of strength and stiffness (e.g., degradation of cementation during shearing) was evaluated across a range of cementation levels. The cementation levels were chosen to represent a broad geologic age range, from young hydraulic fill to Pleistocene sand, as well as different soil class types delineated in the National Earthquake Hazards Reduction Program (NEHRP) site classification (NEHRP 2003). Typical shear wave velocities of the soil states, ages, and behavior were compared to aid the design of the triaxial testing program (Fig. 1). Target shear wave velocities,  $V_s$ , were chosen to represent the following different soil states, ages, and behavior (indicated by the gray bands in Fig. 1): loose, young untreated sand ( $V_s = 180$  m/s, corresponding to NEHRP Site Class E); lightly cemented or aged sand ( $V_s = 300$  m/s, corresponding to NEHRP Site Class D); moderately cemented sand or “very dense soil or soft rock” (from NEHRP site class) ( $V_s = 450$ – $650$  m/s, corresponding to NEHRP Site Class C); and heavily cemented sand or “rock” (from NEHRP site class) ( $V_s = 1,100$ – $1,400$  m/s, corresponding to NEHRP Site Class B). The influence of drained and undrained stress path orientation (i.e., compression, lateral extension, constant mean effective stress) on the stress-strain behavior and cementation degradation of moderately cemented specimens is also presented.

<sup>1</sup>Assistant Professor, Dept. of Civil, Construction, and Environmental Engineering, North Carolina State Univ., Raleigh, NC 27695 (corresponding author). E-mail: bmmorten@ncsu.edu

<sup>2</sup>Professor, Dept. of Civil and Environmental Engineering, Univ. of California, Davis, CA 95616. E-mail: jdejong@ucdavis.edu

Note. This manuscript was submitted on June 27, 2014; approved on January 6, 2015; published online on February 10, 2015. Discussion period open until July 10, 2015; separate discussions must be submitted for individual papers. This paper is part of the *Journal of Geotechnical and Geoenvironmental Engineering*, © ASCE, ISSN 1090-0241/04015019(10)/\$25.00.

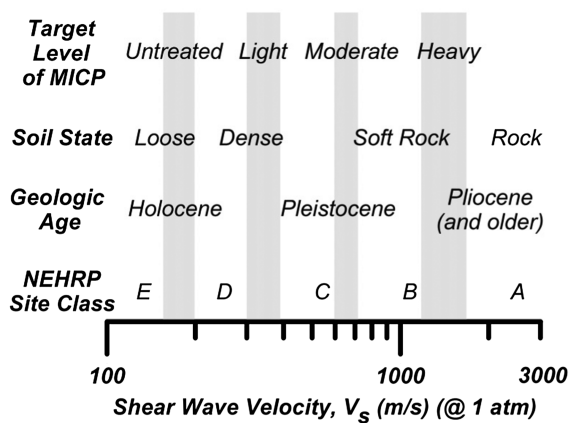


**Fig. 1.** Comparison of target MICP cementation level (indicated with gray bars) to soil state, age, and behavior with approximate shear wave velocity ranges

## Materials and Equipment

### Sand and Specimen Preparation

Triaxial specimens were prepared by dry pluviation to a target relative density of 40% for all loose and treated samples and to 100% for the dense specimen using a calibrated pluviator (DeJong et al. 2006; Jang and Frost 1998). The triaxial specimens had a 72-mm diameter and an aspect ratio of 2:1. Ottawa 50-70 sand was used during this investigation, and a summary of the characteristics of this sand is listed in Table 1. After pluviation, the specimen was placed under vacuum (vacuum of 100 kPa) to apply an effective stress that allowed the specimen to be free standing. The actual diameter and height of the sample were measured once the specimen had been consolidated under the stresses imposed by vacuum, and the relative density was determined for the consolidated state of the specimen. Once the triaxial cell was filled with water, the seating isotropic confining pressure of 100 kPa was slowly applied while the specimen was gradually vented in order for the effective confining stress to not exceeded 100 kPa.

### Biological Treatment Process

The biological preparation and cementation treatment process presented herein is similar to studies by Mortensen et al. (2011) and Martinez et al. (2013). *Sporosarcina pasteurii* [American type culture collection (ATCC) 11859], a urea hydrolyzing bacterium, was grown at 30°C in an ammonium-yeast extract medium [ATCC 1376: 0.13 mol l<sup>-1</sup> Tris buffer (pH = 9.0), 10 g l<sup>-1</sup> (NH<sub>4</sub>)<sub>2</sub>SO<sub>4</sub>, and 20 g l<sup>-1</sup> yeast extract]. Individual ingredients were autoclaved

**Table 1.** Sand Characteristics

Sand property	Sand property values
Sand	Ottawa 50-70
$D_{50}$	0.22 mm
$C_u$	1.4
$C_c$	0.9
$G_s$	2.65
$e_{min}$	0.55
$e_{max}$	0.87
Mineralogy	Quartz
Shape	Round

separately and mixed together poststerilization. The growth medium was inoculated with the *S. pasteurii* stock culture and incubated aerobically at 30°C in a shaking water bath [200 revolutions per minute (rpm)] for approximately 40 h before harvesting at a final optical density (OD<sub>600</sub>) of 0.8–1.0 [600 nm; Pye Unicam PU 8600 ultraviolet/visible light (UV/VIS) spectrophotometer]. Cultures were centrifuged at 4,000g for 20 min in 15 mL volumes, washed in fresh growth medium, and centrifuged a second time. Harvested bacteria were stored in the centrifuge vials at 4°C for a maximum of 14 days.

Urea-calcium chloride cementation media were used to induce ureolytic-driven calcite precipitation. A summary of the components, concentrations, and sterilization methods are presented in Table 2.

Cementation treatments were performed using a peristaltic pump to inject the cementation media at a rate of 10 mL/min into the bottom pore lines of the triaxial equipment. Bacteria were introduced into the soil during the initial cementation injection. Calcium chloride was not included in the initial injection with the bacteria to prevent precipitation during inoculation. Cementation treatments were repeated every 3–6 h. Treatments consisting of two pore volumes of cementation solution (presented in Table 2) were repeated approximately every 3 h until the target  $V_s$  was attained (indicated in Fig. 1). The number of cementation treatments varied, depending on the target  $V_s$ , and ranged from 6 to 16 treatments for the specimens presented herein.

The cementation process was monitored in real time and non-destructively using shear wave velocity. The bender elements used to transmit and receive shear waves across the soil were constructed using special preparation techniques for the highly conductive environmental conditions, including coating the elements with a chemical-resistant, nonconductive sealant (Montoya et al. 2012). The value of  $V_s$  was determined by measuring the travel time required for a 9-V, 100-Hz square wave to travel over a known separation distance between bender elements using a LabView program by Brandenburg et al. (2008).

### Specimen Shearing

Immediately after cementation was completed, the specimen was flushed with a large volume of deaired, deionized water (approximately 10 times the pore volume) in order to remove any remaining salts and air bubbles generated during the cementation process. The specimen was then back-pressured to achieve a minimum  $B$ -value of 0.95. Deaired, deionized water has a slightly acidic pH; therefore, the  $V_s$  of the MICP cemented sand decreased slightly during the saturation process. The  $V_s$  of the specimens reported herein are the values at the end of the saturation and backpressure stage. The isotropic effective confining stress was held constant at 100 kPa until shearing began; the drained tests remained at a confining stress of 100 kPa while the undrained tests developed excess pore pressures during shearing. The drained and undrained triaxial tests were sheared at a rate of 2.5% per hour to a maximum axial strain of 20%. Throughout shearing, the  $V_s$  measurements were used to monitor cementation degradation. For all data presented

**Table 2.** Chemical Recipe for Cementation Media

Chemical	Sterilization	Chemical concentration
Urea	Filter	333 mM
NH <sub>4</sub> Cl	Autoclave	374 mM
NaHCO <sub>3</sub>	Autoclave, dry	0–25.2 mM
Nutrient broth	Autoclave	0–3 g/L
CaCl <sub>2</sub>	Autoclave	50 mM

herein, all measurements are external to the soil sample and are representative of global soil behavior. The strains (volumetric and axial) and shear wave velocities are global measurements, averaged over the entire sample; they do not account for localization.

### Mass of Calcite Measurements

The mass of calcite precipitated by the MICP treatment was determined posttest using a gravimetric acid washing technique. The oven-dried mass of the soil sample was measured before and after an acid wash (5 M HCl). The dissolved calcium carbonate-acid wash solution was rinsed multiple times through a #200 sieve, allowing the dissolved calcium carbonate to be rinsed from the soil while retaining the sand grains. The difference in the two measured masses was taken as the mass of calcite and the percentage of mass of calcite is expressed as the mass of calcite divided by the initial mass of soil (prior to treatment).

### Response of Varying Cementation Levels to Undrained Triaxial Compression

Undrained axial compression triaxial tests were performed to evaluate the improved behavior of MICP treated soil subjected to

undrained loading. For reference, loose untreated sand and dense untreated sand specimens were also subjected to undrained loading (Fig. 2). The shear strength,  $q$ , and excess pore pressure,  $\Delta u$ , have been normalized by the mean effective stress at consolidation,  $p'_c$ , in Fig. 2. A moderately cemented sand with a treated shear wave velocity of 450 m/s exhibited an increase of approximately three times the shear resistance (i.e., difference in effective principal stresses,  $q$ ) of the loose untreated specimen [Fig. 2(b)] as early as approximately 0.5% axial strain. The MICP treated soil also mobilized a greater peak stress ratio ( $q/p'$ ) at low strains [Fig. 2(a)], after which the stress ratio decreased to a value only slightly higher than the untreated loose specimen. The peak stress ratio of the moderately cemented specimen is comparable to that of the dense sand specimen; however, the treated soil exhibited strain softening of the stress ratio after the peak stress ratio is reached while the dense sand did not. The absolute shearing resistance ( $q$ ) for both specimens was, however, strain hardening. Normalized excess pore pressures ( $\Delta u/p'_c$ ) [Fig. 2(c)] for the treated and dense sand specimens indicate similar negative pore pressure development to a strain of approximately 1%, above which the dense sand generates much higher negative pressures. The treated sand exhibits dilative tendencies, possibly because the brittle cementation between particle-particle contacts forces localized dilation within the shear band.

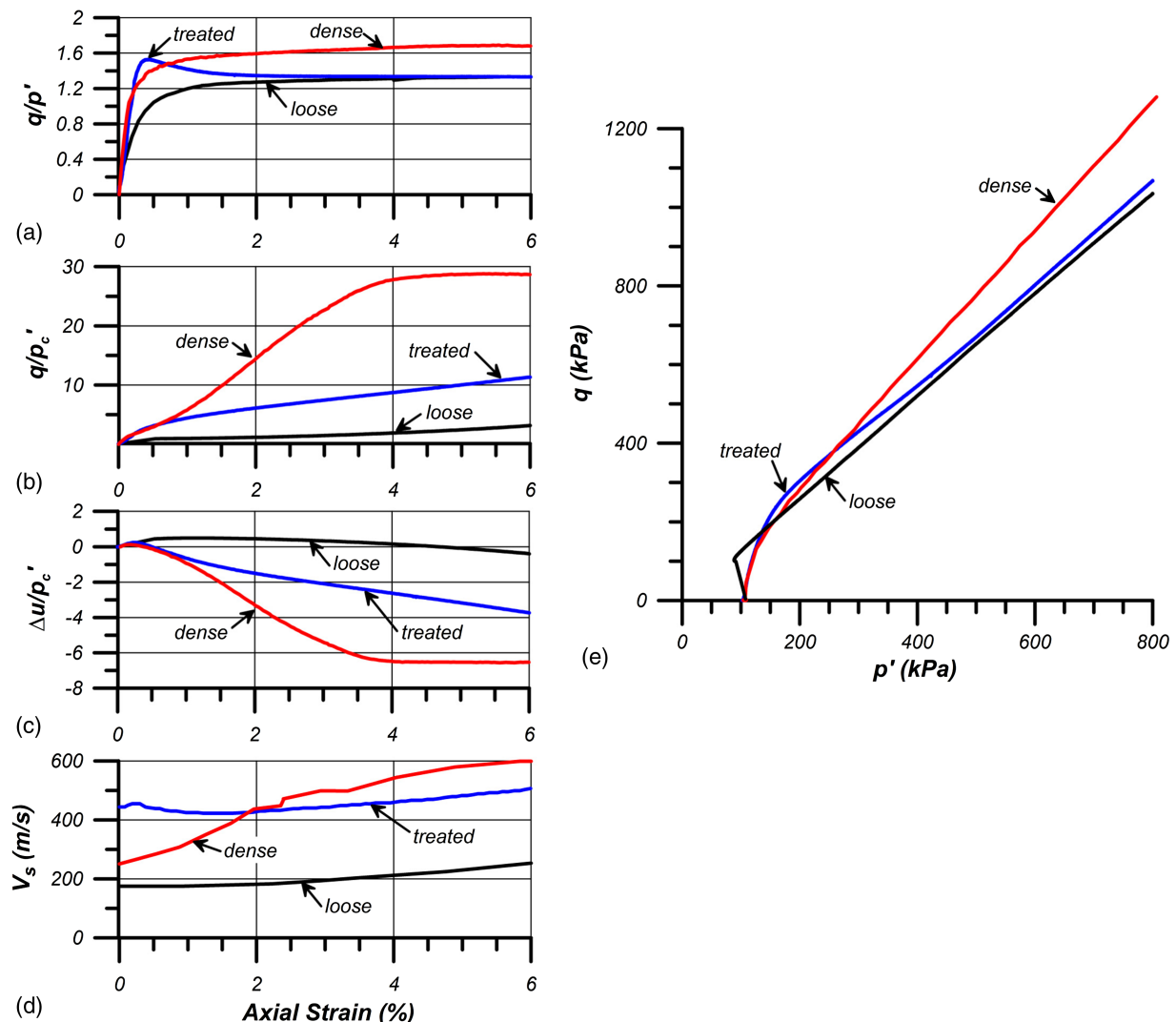
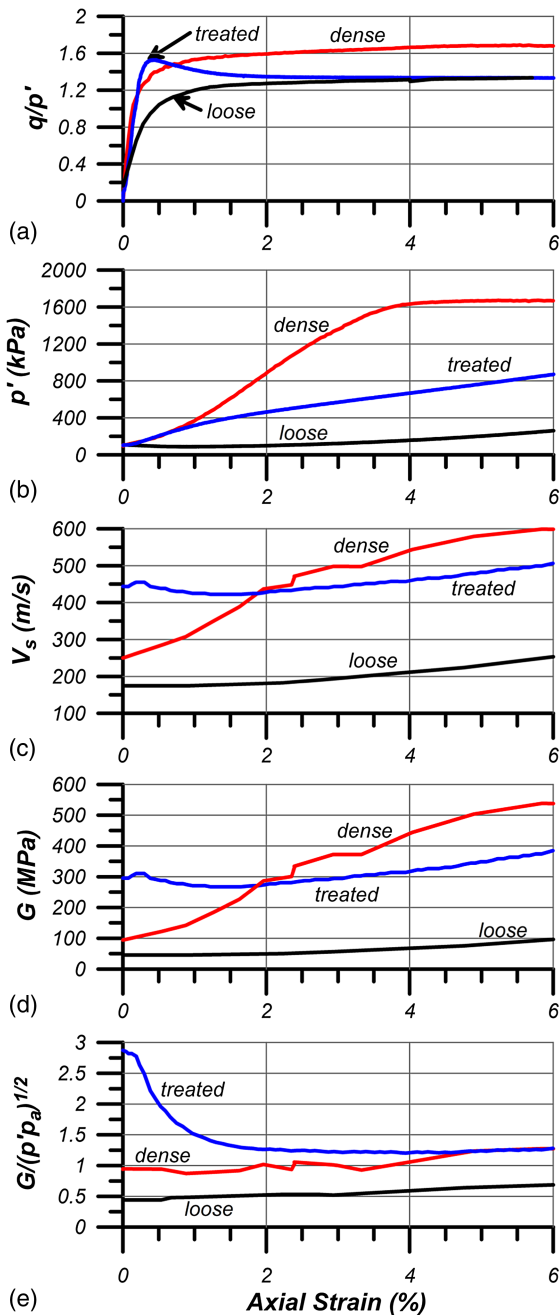


Fig. 2. Undrained triaxial compression tests of MICP treated ( $V_s = 450$  m/s) and untreated specimen



**Fig. 3.** Normalized shear modulus behavior subjected to undrained loading to illustrate cementation degradation by removing the effect of changing confinement from negative pore pressure generation

The normalized excess pore pressures for the loose untreated specimen exhibits contractive tendencies until strains of approximately 4.5%, after which negative excess pore pressures developed.

The shear wave velocity evolves during undrained shearing due to a combination of cementation degradation as well as an increase in mean effective confining stress ( $p'$ ) due to the increase in axial stress and the negative pore pressure generation [Fig. 2(d)]; the change in mean effective stress during shearing is illustrated in Fig. 3. For example, the shear wave velocity of the dense sand increases with shearing because of the increase in  $p'$ ; however, the shear wave velocity of the treated sand remains relatively constant because the cementation is degrading at the same time that  $p'$  is increasing. In order to isolate cementation degradation, the

**Table 3.** Stiffness and Strength Parameters for Treated Soil

Triaxial test	Initial $D_r$ (%)	Initial $V_s$ (m/s)	Mass of calcite (%)	Peak $q/p'$	$G$ (MPa)	$\phi'_{peak}$
Loose untreated	37	190	0	1.30	54	33.0
Dense untreated	101	250	0	1.69	100	40.0
Light cementation	34	300	1.01	1.33	135	33.6
Moderate cementation	40	450	<sup>a</sup>	1.53	304	37.4
Moderate cementation	33	650	1.30	1.63	634	39.2
Heavy cementation	31	1,100	3.06	1.77	1,815	41.5
Heavy cementation	45	1,400	5.31	1.91	2,940	43.7

<sup>a</sup>No mass of calcite information.

influence of the increasing confining stress was removed by normalizing the shear modulus,  $G$ , to the square root of the mean effective stress of the soil specimen,  $p'$ . The square root of  $p'$  was used to normalize  $G$  because the shear modulus is approximately proportional to the square root of the mean effective stress in sands (Stokoe et al. 1985). The normalized shear modulus,  $G/(p'p_a)^{1/2}$ , indicates that the cementation begins to rapidly degrade once the peak shear stress ratio is reached (approximately 0.25% strain) (Fig. 3). The normalized shear modulus is also relatively constant during shearing of the untreated soils, both loose and dense, as expected.

Five specimens prepared at different levels of MICP cementation, summarized in Table 3, were subjected to isotropic consolidated undrained compression loading to examine the influence of cementation level on stress-strain behavior. The tests indicate that the maximum shear strength ( $q$ ) at small strains (less than 3% axial strain) and the maximum stress ratio ( $q/p'$ ) increase as the cementation increases (Fig. 4 and tabulated in Table 3). At larger strains, there is a transition from strain hardening to strain softening behavior as the cementation increases. The stress-strain behavior indicates that the specimens with high cementation levels ( $V_s > 650$  m/s) reach a peak shear strength ( $q$ ) value and then begin to soften as cementation degrades within a defined shear zone. Specimens with lower levels of cementation (at  $V_s$  of 450 m/s and lower) as well as the untreated loose specimen continue to strain harden. The transition between strain hardening and strain softening appears to occur around a shear wave velocity of 650 m/s; the test performed at this shear wave velocity has a very subtle strain hardening behavior [Fig. 4(b)]. The implication of this transition in behavior is that at higher strain levels (e.g., above 4% axial strain) the 450 m/s specimen has a higher shear strength ( $q$ ) than the 650 m/s specimen. The observed transition in stress-strain behavior corresponds to a transition from a global failure to a narrow, defined shear band. As illustrated in Fig. 5, as the cementation increases, the sheared soil is concentrated to narrower zones of the specimen.

The stress ratio behavior [Fig. 4(a)] indicates that the lightly and moderately cemented sands tend to converge towards the untreated loose sand at high strain levels, indicating that the critical state stress ratios of the treated loose sand are similar to those for the untreated loose sand. As discussed in DeJong et al. (2010), the actual critical state stress ratio of the treated soils is likely slightly different than the untreated soil because of the added calcite mass (manifested as fines and increased particle roughness at large strains). In addition, the strain at which the maximum stress ratio is reached also generally decreases with increasing cementation. The exception in the data presented herein is the moderately cemented sand ( $V_s = 650$  m/s) where the peak stress ratio was reached at lower strains than the heavily cemented sands. The moderately cemented sand appears to be an anomaly relative to the

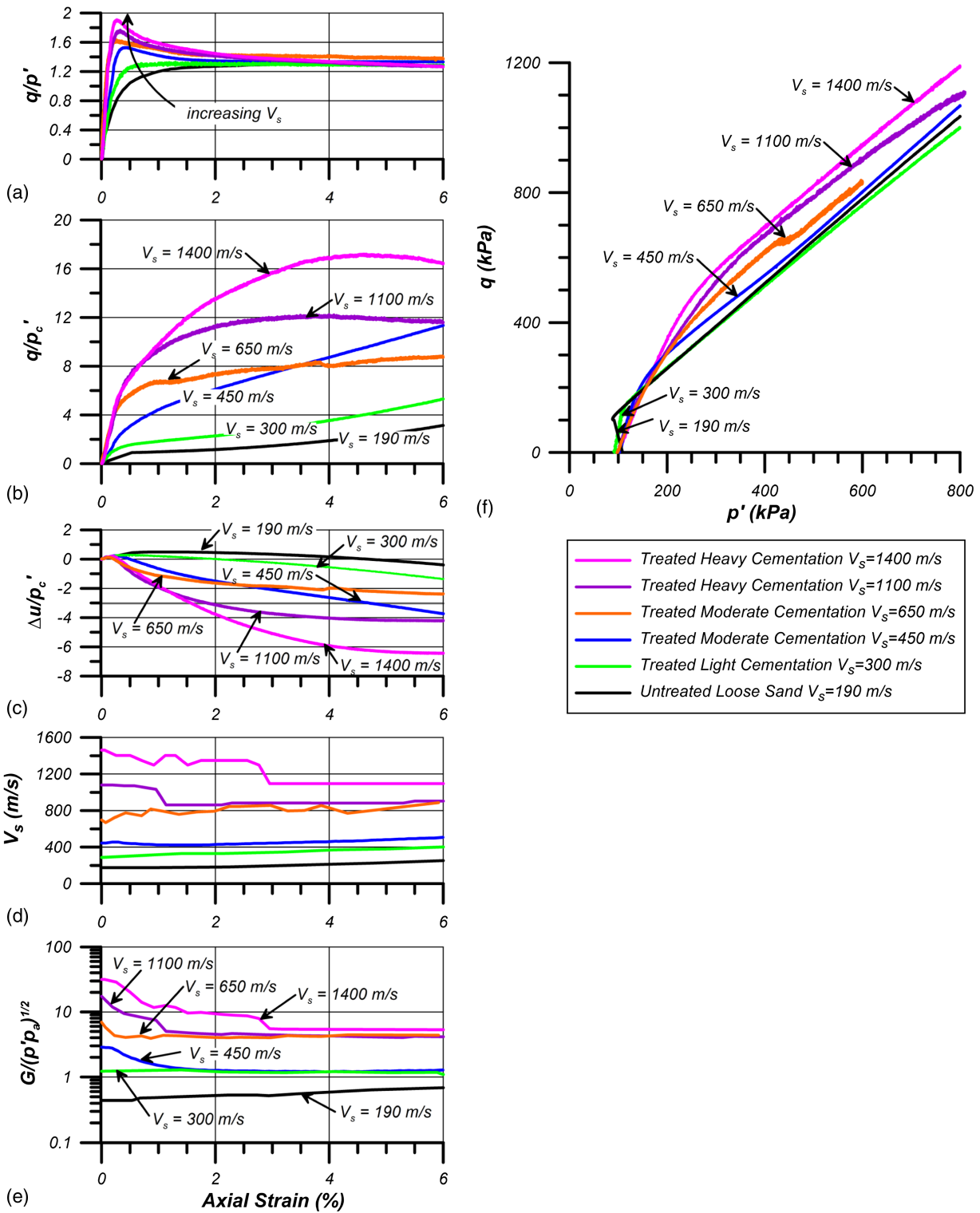


**Fig. 4.** Normalized undrained triaxial shearing and shear wave velocity measurements of five MICP treated soils at varying levels of cementation (indicated in the legend)

other tests; at a shear stress of about 650 kPa and an axial strain of approximately 1–1.5%, the shear strength degrades and begins to approach the critical state line in the  $q$ - $p'$  space [Fig. 4(f)].

Normalized excess pore pressure [Fig. 4(c)] of all the treated soils followed similar trends previously discussed (Fig. 2). The treated soils with shear wave velocities of 450 m/s or greater have similar dilative tendencies as the dense untreated sand (Figs. 2 and 4). The lightly cemented sand with an initial shear wave velocity of

300 m/s behaves like a transitional material between the untreated loose sand and the moderately cemented sand, as expected. The lightly cemented sand experiences positive pore pressures upon loading until approximately 2.0% strain, when the lightly cemented sand begins to generate negative pore pressures with continued shearing.

The evolution in the measured shear wave velocity of the moderately and lightly cemented sand specimens during undrained

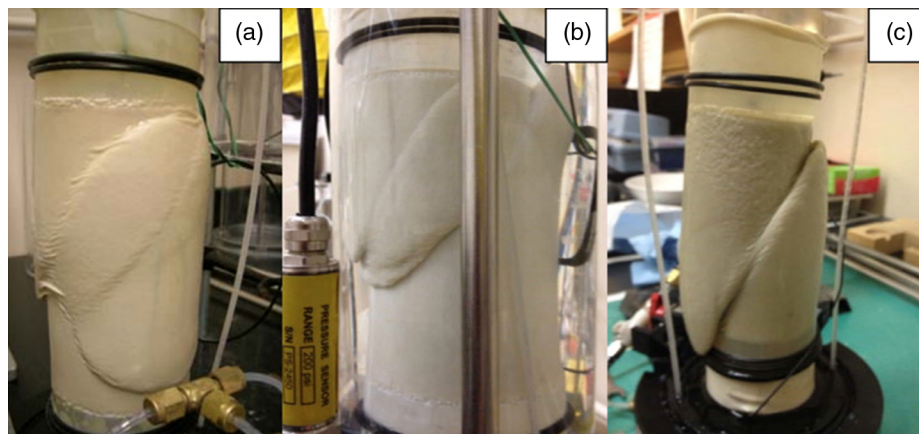


**Fig. 5.** Final (e.g., at 20% strain) shear bands of three of the isotropically consolidated undrained compression (ICUC) triaxial tests performed at shear wave velocities of (a) 450; (b) 650; and (c) 1,400 m/s, as the photos indicate, the shear zone becomes more defined and concentrated as the shear wave velocity increases

shearing are a combination of cementation degradation as well as increasing effective confinement [Fig. 4(c)]; however, the measured  $V_s$  of the heavily cemented sand is less influenced by the increase in confinement. At the heavily cemented levels (e.g., 1,100–1,400 m/s), the shear wave velocity decreases with the development of a shear band (visually observed between 1 and 3% strain) and then remains relatively constant with continued shearing. This shear wave velocity trend is attributed to the shear wave velocity being a bulk measurement across the entire height of the specimen, and only a small proportion of the cementation degrades within the shear band while most of the cemented bonds within the specimen remain undamaged. Also, the shear wave velocity of the highly cemented specimens are more strongly affected by the cementation than by the value of  $p'$  [further discussed in Montoya et al. (2013)].

Finally, the undrained triaxial shear results indicate an increase in equivalent effective friction angle with increase in cementation (Table 3 and Fig. 6). Given one test per cementation level, the effective friction angle was approximated assuming a cohesive intercept equal to zero for the Mohr-Coulomb failure criteria. This is a simplification because MICP cementation at levels corresponding to shear wave velocity levels of approximately 1,000 m/s and higher enable specimens to retain their shape under self-weight. The assumption that the cohesive intercept is zero and the increase in shear strength is due to an increase in the frictional component represents different behavior compared with other artificially cemented sands (Clough et al. 1981). However, the assumption is reasonable for MICP cemented sands at lower cementation levels (as further confirmed subsequently in drained triaxial test results). The peak effective friction angle of the untreated loose and dense sand specimens was 33 and 40°, respectively. The moderately and heavily cemented sand (specimen at and above  $V_s = 450$  m/s) have an approximate linear relationship between the effective friction angle and the shear wave velocity. The lightly cemented sand ( $V_s = 300$  m/s) is outside the linear relationship of the other treated soils; the effective friction angle is slightly greater than the untreated loose sand (33.6°).

## Response to Varying Load Paths

### Response to Drained Loading under Varying Load Paths

Drained triaxial tests were performed on MICP treated samples to compare the improved drained strength from MICP treatment with a baseline untreated specimen and to compare the evolution in

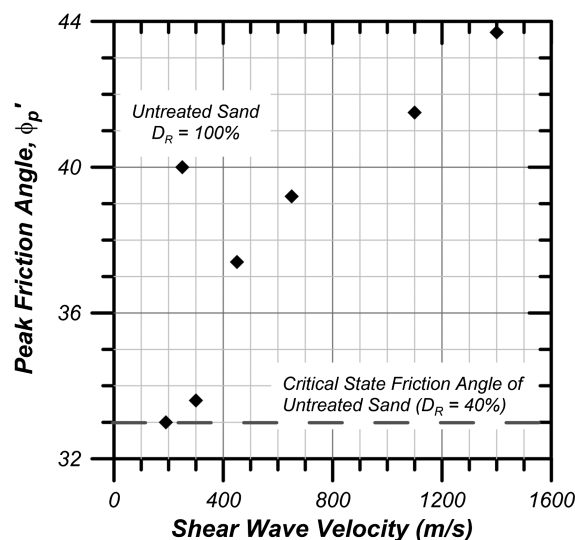


**Fig. 6.** Peak effective friction angle as it is related to the specimen cementation level, measured using shear wave velocity

strength and stiffness of the cemented specimen subjected to different loading paths. The treated specimens subjected to drained loading were all treated to a moderate cementation level with a  $V_s$  of approximately 450 m/s. For comparison, the baseline untreated specimens had an initial  $V_s$  of approximately 180 m/s.

The behaviors of the drained axial compression triaxial tests for the MICP treated and untreated loose sand specimens are compared to examine the influence of cementation on the stress-strain behavior (Fig. 7). The MICP treated specimen exhibits an increase of approximately 1.3 times the peak shear strength of the loose untreated specimen [Fig. 7(a)]. After reaching the peak shear strength, the drained MICP specimen slowly softens as the cementation degrades with continued shearing. Shear strengths at large strains are similar for both the MICP treated and untreated specimens. The  $V_s$  data indicate that the cementation in the MICP treated specimen continues to degrade throughout shearing and that the  $V_s$  approaches that of the untreated specimen at large strains [Fig. 7(b)]. Using the bulk  $V_s$  measurements at large strain and assuming the soil outside of the shear band does not degrade (shear

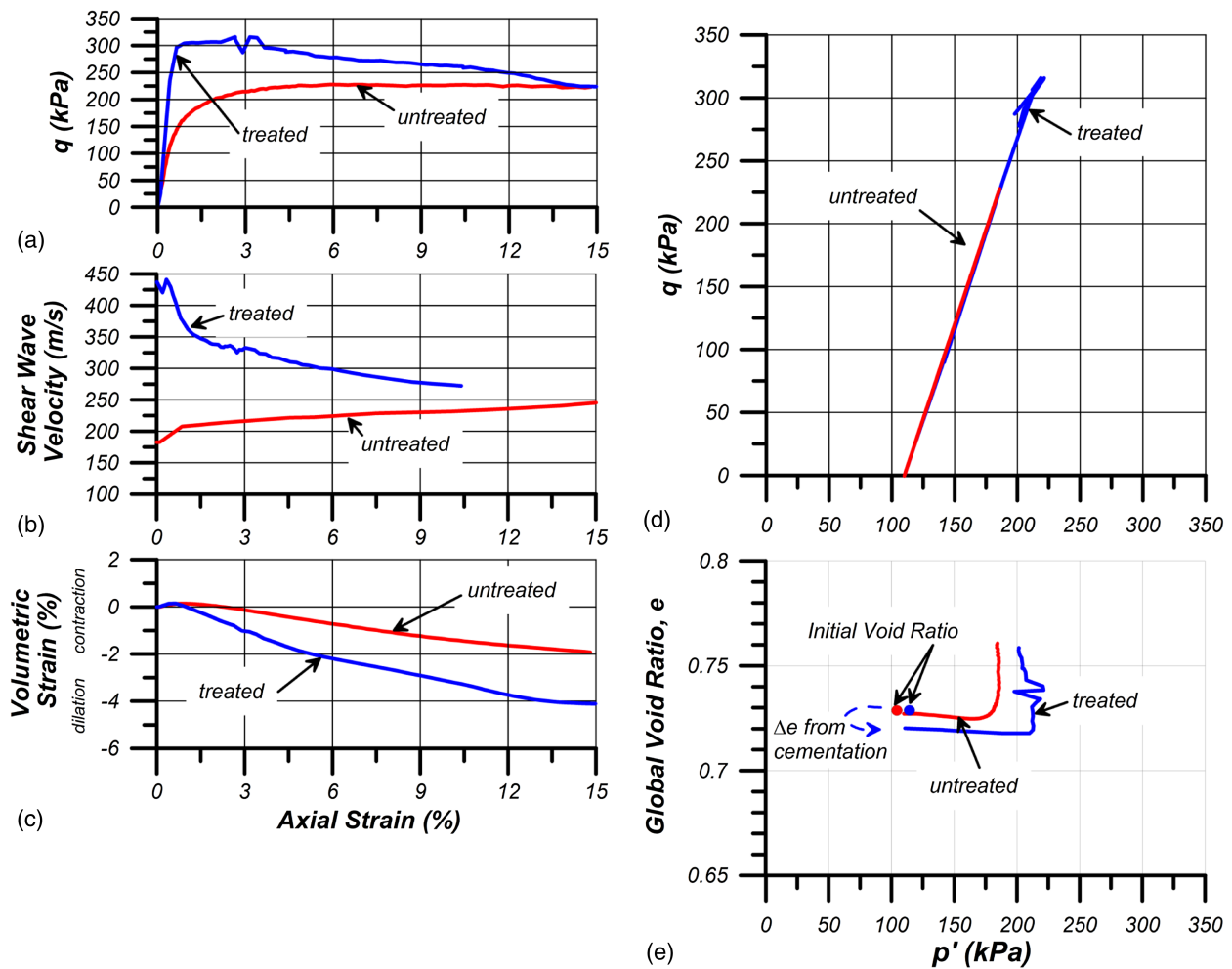


**Fig. 7.** Drained triaxial compression tests of MICP treated and untreated specimen; the initial void ratios of the two specimen prior to cementation were equivalent ( $e = 0.73$ ); the change in void ratio from the cementation (mass of calcite measured to be 0.6% by mass) was estimated assuming a density of calcite of  $1.62 \text{ g/cm}^3$  (Weil et al. 2012); the initial void ratio of the treated sample prior to shearing was estimated to be 0.72

band estimated to be 43 mm based on photographs), the shear wave velocity of the sand within the shear band of the cemented sample is approximately 180 m/s, which is similar to that of loose untreated sand. Additionally, the volumetric behavior changes with precipitated calcite; the treated sample exhibits dilation while the untreated sample undergoes contraction. This behavior agrees with that discussed previously of the MICP treated specimens subjected to undrained loading generating negative excess pore pressures.

Several moderately cemented samples ( $V_s = 450 \text{ m/s}$ ) were each sheared under different drained loading paths: axial compression ( $\sigma_1$  increases while  $\sigma_3$  held constant), radial extension ( $\sigma_3$  decreases while  $\sigma_1$  held constant), and constant  $p$  with increasing  $q$  (where  $p$  is the average of  $\sigma_1$ ,  $\sigma_2$ , and  $\sigma_3$ ). The drained peak shear strength and behavior of the cemented sand are influenced by the loading path (Fig. 8). The cemented specimen subjected to a radial extension load path reached the peak shear strength at very small strains (approximately 0.1% strain). In contrast, the cemented specimen subjected to an axial compression load path reached the peak strength at a larger strain (approximately 1% strain). The cemented specimen subjected to a constant  $p$  load path reached the peak shear strength at a strain level between the other two loading paths (approximately 0.2% strain after  $q$  begins to increase). The shear strength data indicate that as the loading path transitions from

increasing  $p'$  to decreasing  $p'$ , the shear behavior begins to become more brittle. Neglecting lode angle dependency for simplicity, the results in Fig. 8 can be used to develop the failure envelopes corresponding to both peak stress ratios and large-strain critical state conditions (20% strain). These results suggest that the failure envelopes are predominantly frictional with a minimal portion of the strength increase attributed to cohesion at these levels of MICP cementation. The peak failure envelope appears to be a slightly curved line with a small amount of cohesion. The critical state envelope, in  $p'$ - $q$  space, is a relatively straight line with no cohesion.

The degradation of cementation during shearing was again monitored with shear wave velocity measurements [Fig. 8(b)]. Degradation of the cementation, marked by a decrease in shear wave velocity, follows similar patterns to the drained shear response. The cementation of the specimen subjected to radial extension begins to degrade immediately upon loading; the degradation of  $V_s$  is fastest for this loading path because the cementation is degrading and  $p'$  is decreasing at the same time. Similarly, cementation in the specimen subjected to a constant  $p$  loading path degrades when  $q$  begins to increase (corresponding to approximately 0.1% strain in Fig. 8), which occurs slightly before the peak shear strength is reached. Degradation of  $V_s$  for this specimen can be attributed to degradation of cementation alone. Similar behavior

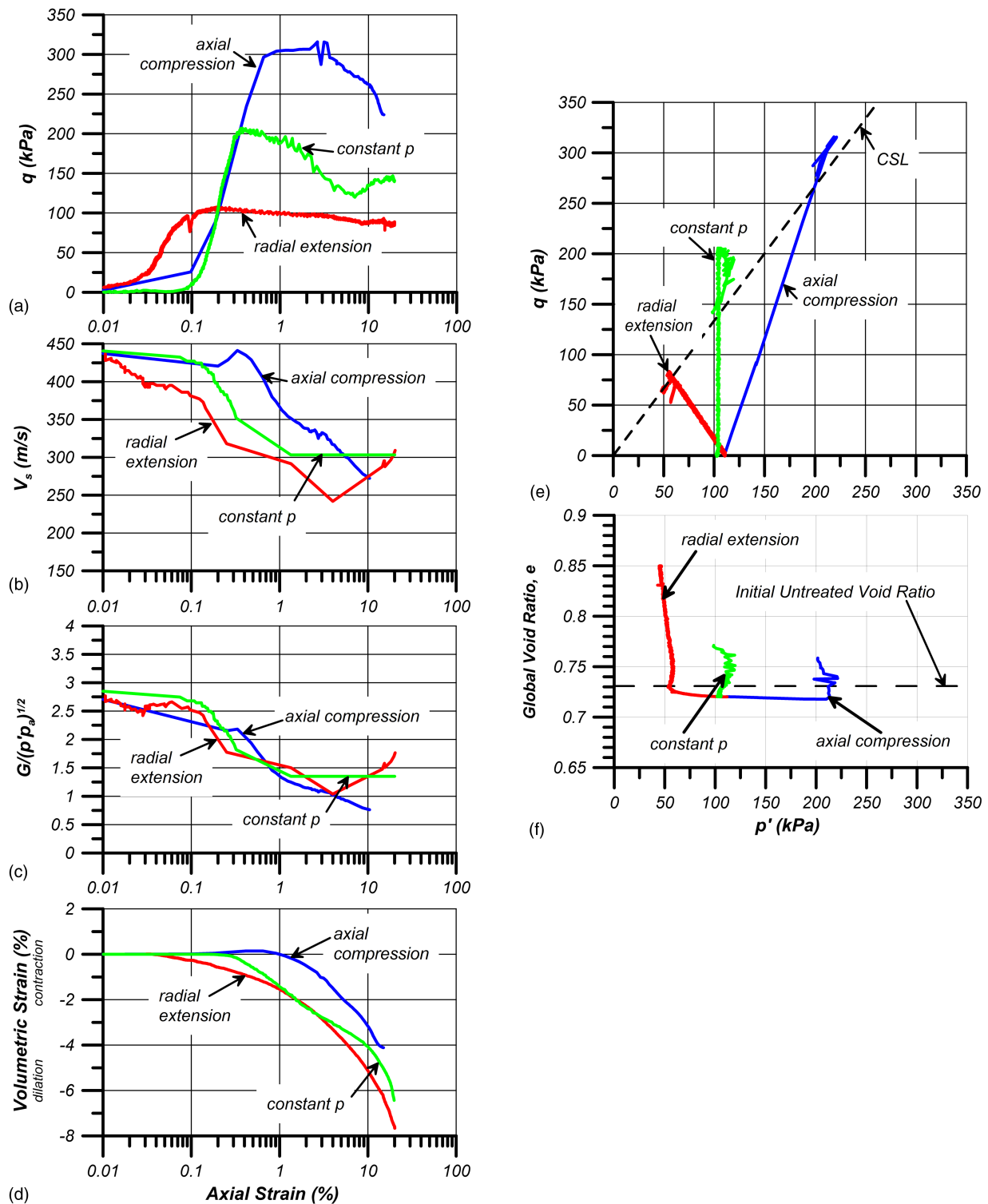


**Fig. 8.** Drained triaxial tests, with varying loading paths, performed on moderately cemented samples ( $V_s$  approximately 450 m/s); the axial strains are plotted on a log scale to expand the behavior at small strains (less than 0.1%)

is exhibited in the cemented specimen subjected to axial compression. The cementation degradation begins at approximately 0.3% strain under axial compression. The rate and amount of degradation in  $V_s$  is smallest for this loading path because the degradation of the cementation is counterbalanced by the increasing  $p'$ . The normalized shear modulus,  $G/(p' p_a)^{1/2}$  [Fig. 8(c)] indicates that the rate of cementation degradation is similar for all three loading paths.

### Response to Undrained Loading under Varying Load Paths

Three MICP treated specimens were subjected to undrained shear under different loading paths (Fig. 9), similar to the drained test series described previously. The test results indicate that as with the drained specimens, the total stress path influences the constitutive behavior of the cemented soil with small deviations in the

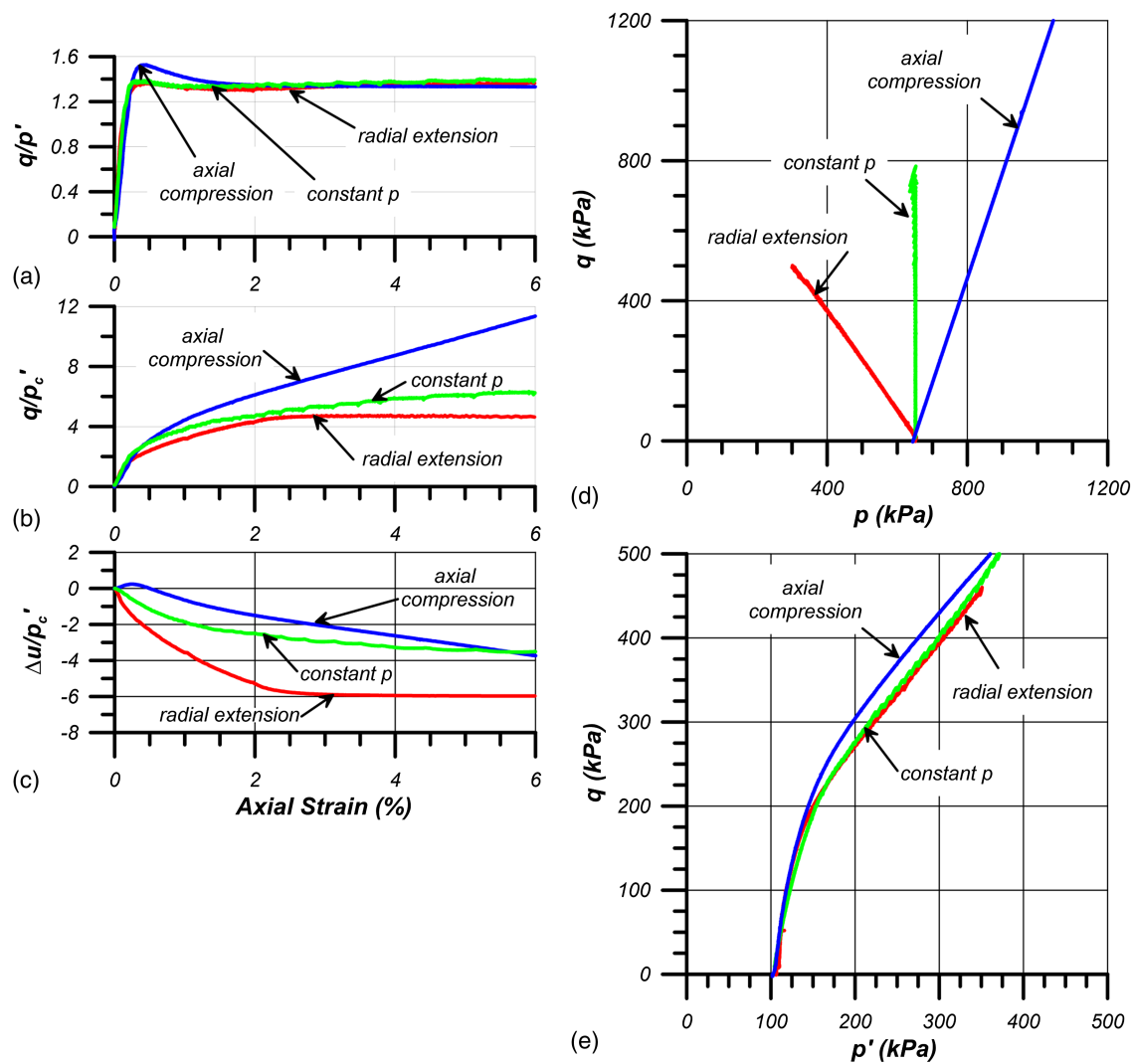


**Fig. 9.** Undrained triaxial tests, with varying total stress loading paths, performed on moderately cemented samples ( $V_s$  approximately 450 m/s); the final strains reached for the preceding tests were an axial strain of 20% for the radial extension and constant  $p$  tests; the axial compression test was terminated at an axial strain of approximately 7% due to cavitation

effective stress paths [Fig. 9(c)]. These results appear appropriate considering that the specimens' behavior should be bracketed between that of uncemented sand and fully cemented sand subjected to undrained loading. The behavior of undrained, uncemented sand would be independent of the three total stress paths used, resulting in equivalent effective stress paths; however, the response of fully cemented sand would be entirely dependent on the total stress path. The response of the moderately cemented sands indicates that the soil strength ( $q$ ) is slightly dependent on the total stress path, even if the influence is subtle at this low level of cementation (initial  $V_s = 450$  m/s for all three specimens).

The stress-strain behavior at low strain (less than 2.5%) is similar but not equivalent for the three different total stress loading paths. The shear strength ( $q$ ) behavior is only compared at low strains because of the loss of saturation due to cavitation in the radial extension test at approximately 2.5–3.0% axial strain. The specimen subjected to the radial extension and constant  $p$  loading paths exhibited similar stress-strain behavior, while the specimen subjected to an axial compression load path mobilized higher peak shear strength. The stress ratio for all three specimens exhibited strain softening behavior and had similar residual stress ratio values. The peak stress ratio was mobilized at a similar strain for all

three specimens. The similar shearing behavior (e.g., similar strain levels at peak stress ratio) is due to the similar effective stress paths, even though there is a minor influence from the different total stress paths.

Strong negative pore pressures developed in all tests, with the specimen subjected to the radial extension loading path exhibiting the largest negative pressures and the specimen subjected to the axial compression loading path exhibiting the lowest negative pressures of the three tests. The changes in pore pressure are due to both a change in mean total stress and to volume change tendencies of the soil. Because the radial extension path produced the greatest reduction in  $p$ , very large negative pore pressures developed, which lead to cavitation despite the initial backpressure and saturation level ( $u_o = 550$  kPa and  $B = 0.98$  prior to shearing). Once the sample was no longer saturated, the loading was no longer undrained and the shear strength ( $q$ ) leveled off with increased shearing [Fig. 9(c), 2.5–3.0% axial strain].

## Conclusions

The shear strength and stiffness of the MICP treated soils dramatically improve with an increase in MICP cementation. As the

cementation increased, determined using shear wave velocity, the peak shear stress ratio increased and the peak ratio was reached at lower axial strains when subjected to undrained loading. The peak stress ratio,  $q/p'$ , increased from the loose untreated sand value of 1.3 up to 1.9 for cemented sand with a shear wave velocity of 1,400 m/s. The critical state stress ratio was not significantly affected by the cementation. The peak shear strength ( $q$ ) increased with the increase in cementation level, and as the cementation increased the stress-strain behavior transitioned from strain hardening to strain softening. The addition of the MICP cementation also increased the dilatancy of the loose sand.

The loading path influences the behavior of the MICP treated specimen as shown in both drained and undrained triaxial shear behavior. The rate of stiffness reduction due to cementation degradation prior to failure as well as the subsequent softening was also shown to depend on the effective stress path and drainage condition dependent. Shear wave velocity monitoring was successful in capturing cementation degradation as well as changes in confinement ( $p'$ ). Normalizing the shear modulus by the confinement effective stress enabled separation of the effects of changes in  $p'$  and cementation level. The success of using shear wave velocity to monitor both the mineral precipitation process and the cementation degradation indicates that shear wave velocity is a valuable technique for process monitoring as MICP is upscaled towards field implementation. Shear wave velocity may be essential for verification of MICP cementation during the treatment phase and also used to monitor the level of cementation after loading has occurred (e.g., an earthquake).

## Acknowledgments

Funding from the National Science Foundation (#0727463 and #0830182) is appreciated. Any opinions, findings, and conclusions or recommendations expressed in this material are those of the writer(s) and do not necessarily reflect the views of the National Science Foundation.

## References

- Brandenberg, S. J., Kutter, B. L., and Wilson, D. W. (2008). "Fast stacking and phase corrections of shear wave signals in a noisy environment." *J. Geotech. Geoenviron. Eng.*, 10.1061/(ASCE)1090-0241, 1154–1165.
- Chou, C. W., Seagren, E. A., Aydilek, A. H., and Lai, M. (2011). "Biocalcification of sand through ureolysis." *J. Geotech. Geoenviron. Eng.*, 10.1061/(ASCE)GT.1943-5606.0000532, 1179–1189.
- Clough, G. W., Sitar, N., and Bachus, R. C. (1981). "Cemented sands under static loading." *J. Geotech. Eng.*, 107(GT6), 799–817.
- DeJong, J. D., et al. (2013). "Biogeochemical processes and geotechnical applications: Progress, opportunities, and challenges." *Geotechnique*, 63(4), 287–301.
- DeJong, J. T., et al. (2011). "Soil engineering in vivo: Harnessing natural biogeochemical systems for sustainable, multi-functional engineering solutions." *J. R. Soc. Interface*, 8(54), 1–15.
- DeJong, J. T., Fritzges, M. B., and Nüsslein, K. (2006). "Microbial induced cementation to control sand response to undrained shear." *J. Geotech. Geoenviron. Eng.*, 10.1061/(ASCE)1090-0241(2006)132:11(1381), 1381–1392.
- DeJong, J. T., Mortensen, B. M., Martinez, B. C., and Nelson, D. C. (2010). "Bio-mediated soil improvement." *Ecol. Eng.*, 36(2), 197–210.
- Fujita, Y., et al. (2008). "Stimulation of microbial urea hydrolysis in groundwater to enhance calcite precipitation." *Environ. Sci. Technol.*, 42(8), 3025–3032.
- Ivanov, V., and Chu, J. (2008). "Applications of microorganisms to geotechnical engineering for bioclogging and biocementation of soil in situ." *Rev. Environ. Sci. Biotechnol.*, 7(2), 139–153.
- Jang, D.-J., and Frost, J. D. (1998). "Sand structure differences resulting from specimen preparation procedures." *Geotechnical earthquake engineering and soil dynamics III*, Geo-Institute of ASCE, Reston, VA, 234–245.
- Karol, R. H. (2003). *Chemical grouting and soil stabilization*, Marcel Dekker, New York.
- Martinez, B. C., et al. (2013). "Experimental optimization of microbial induced carbonate precipitation for soil improvement." *J. Geotech. Geoenviron. Eng.*, 10.1061/(ASCE)GT.1943-5606.0000787, 587–598.
- Mitchell, J. K., and Santamarina, J. C. (2005). "Biological considerations in geotechnical engineering." *J. Geotech. Geoenviron. Eng.*, 10.1061/(ASCE)1090-0241(2005)131:10(1222), 1222–1233.
- Montoya, B. M., et al. (2012). "Fabrication, operation, and health monitoring of bender elements for aggressive environments." *Geotech. Test. J.*, 35(5).
- Montoya, B. M., DeJong, J. T., and Boulanger, R. W. (2013). "Seismic response of liquefiable sand improved by microbial induced calcite precipitation." *Geotechnique*, 63(4), 302–312.
- Mortensen, B. M., Haber, M. J., DeJong, J. T., Caslake, L. F., and Nelson, D. C. (2011). "Effects of environmental factors on microbial induced calcium carbonate precipitation." *J. Appl. Microbiol.*, 111(2), 338–349.
- NEHRP (National Earthquake Hazards Reduction Program). (2003). "Recommended provisions for seismic regulations for new buildings and other steel structures. Part 1: Provisions." Federal Emergency Management Agency, 338.
- Stocks-Fischer, S., Galinat, J. K., and Bang, S. S. (1999). "Microbiological precipitation of CaCO<sub>3</sub>." *Soil Biol. Biochem.*, 31(11), 1563–1571.
- Stokoe, K. H., Lee, S. H. H., and Knox, D. P. (1985). "Shear moduli measurements under true triaxial stresses." *Advances in the art of testing soils under cyclic conditions*, V. Khosla, ed., ASCE, Detroit, 166–185.
- van Paassen, L. A., Ghose, R., van der Linden, T. J. M., van der Star, W. R. L., and van Loosdrecht, M. C. M. (2010). "Quantifying biomediated ground improvement by ureolysis: Large-scale bio-grout experiment." *J. Geotech. Geoenviron. Eng.*, 10.1061/(ASCE)GT.1943-5606.0000382, 1721–1728.
- Weil, M. H., DeJong, J. T., Martinez, B. C., and Mortensen, B. M. (2012). "Seismic and resistivity measurements for real-time monitoring of microbial induced calcite precipitation in sand." *Geotech. Test. J.*, 35(2), 330–341.
- Whiffin, V. S., van Paassen, L. A., and Harkes, M. P. (2007). "Microbial carbonate precipitation as a soil improvement technique." *Geomicrobiol. J.* 24(5), 417–423.